MATERIALS CHEMISTRY
FRONTIERS

RESEARCH ARTICLE

View Article Online
View Journal | View Issue

Cite this: *Mater. Chem. Front.*, 2021, **5**, 1995

Synergistic effects of the zinc acetate additive on the performance enhancement of Sn-based perovskite solar cells†

Guanqi Tang,‡ Sihua Li,‡ Jiupeng Cao, Tianyue Wang, Peng You, Qidong Tai and Feng Yan *

Received 10th December 2020,
Accepted 2nd January 2021

DOI: 10.1039/d0qm01036g

rsc.li/frontiers-materials

Tin-based perovskites are promising candidates for preparing lead-free perovskite solar cells due to the optimal bandgap and excellent optoelectronic properties, while the low formation energy of Sn^{2+} vacancy and facile oxidation of Sn^{2+} to Sn^{4+} lead to low efficiency and poor air instability of tin-based PSCs. Here, zinc acetate ($ZnAc_2$) is employed as an additive to form a $FAI{\cdot}SnI_2{\cdot}ZnAc_2$ intermediate phase in the as-deposited films and control the crystallization process. Besides, the presence of Zn ions could favor the crystal growth by modifying the nucleation process. These synergistic effects lead to high-quality tin-based perovskite films with a large grain size and a low density of Sn^{2+} vacancies. Moreover, $ZnAc_2$ could form a complex with $SnCl_2$ and an antioxidant to uniformly encapsulate the grains and further improve the air stability of the perovskite layers. As a result, the efficiency of tin-based perovskite solar cells is improved from 6.70% to 8.38%. This work demonstrates a viable strategy to fabricate highly efficient and air-stable Sn PSCs by simultaneously suppressing the formation of Sn^{2+} vacancy and oxidation of Sn^{2+} in perovskite films.

Introduction

Organic–inorganic lead halide perovskite solar cells (PSCs) have achieved a certified power conversion efficiency (PCE) of 25.5%, which rival commercial silicon solar cells.[1] However, the toxic lead contained in state-of-the-art PSCs is a big environmental threat to real-life applications due to its water solubility and easy uptake by plants.[2–7] Therefore, eco-friendly lead-free perovskites are desired for future commercialization of perovskite photovoltaic technologies. Recently, various lead-free perovskites have been explored, such as tin (Sn),[8–12] germanium (Ge),[13,14] bismuth (Bi),[15,16] and antimony (Sb).[17,18] Among them, tin-based perovskites have a similar crystal structure to lead counterparts, an optimal bandgap (1.2–1.4 eV) close to the Shockley–Queisser limit, high carrier mobility and low exciton energy, which enable great potential for high efficiency lead-free PSCs.[19–23] However, the PCE of tin-based PSCs is much lower than that of lead-based analogs.[24]

The relatively lower efficiency of tin-based PSCs compared with lead counterparts is ascribed to the intrinsic chemical instability of Sn^{2+} and difficulty in controlling the morphology of perovskite films due to the fast crystallization.[21] The low formation energy of Sn^{2+} vacancy in the crystallization process and the easy oxidation of Sn^{2+} to Sn^{4+} upon air exposure lead to the higher carrier recombination and metallic behavior of tin-based perovskite films due to high hole density.[25] The fast crystallization due to the strong Lewis acidity of Sn^{2+} results in poor-quality perovskite films with pin holes and randomly oriented crystals.[26,27] Hence, some strategies are explored to increase the formation energy of Sn^{2+} vacancy and prevent the oxidation of Sn^{2+} *via* composition engineering[28–35] and additive introduction.[12,36–40]

Recently, our group reported techniques for the *in situ* encapsulation of tin-based perovskite grains by introducing antioxidants (hydroxybenzene sulfonic acid and gallic acid), which could effectively prolong the air lifetime of tin-based PSCs.[39,41] Although the oxidation of Sn^{2+} by outer oxygen is highly suppressed, the intrinsic Sn^{2+} vacancy in perovskite films, especially at grain boundaries, is not effectively alleviated due to the decreased grain size by the introduction of antioxidant additives, which limits further efficiency improvement. Therefore, a new strategy is needed to control the crystallization process to further decrease Sn^{2+} vacancies to improve the efficiency of our tin-based PSCs.

Herein, a small amount of zinc acetate ($ZnAc_2$) is introduced into our perovskite precursors to control the crystallization

Department of Applied Physics, The Hong Kong Polytechnic University, Hong Kong, P. R. China. E-mail: apafyan@polyu.edu.hk

† Electronic supplementary information (ESI) available. See DOI: 10.1039/d0qm01036g

‡ These authors contributed equally to this work.

process during film deposition. It is found that the grain size of perovskite films is enlarged and defect density is efficiently suppressed, which can be ascribed to the following two effects. First, a FAI·SnI_2·$ZnAc_2$ intermediate phase is formed during the crystallization process due to the strong bonding of the Lewis base group of Ac^- and the Lewis acid of Sn^{2+}. This intermediate phase could avoid the loss of Sn^{2+} during the crystallization process and also retard the crystallization process. Second, Zn ions can modify the nucleation and crystal growth processes. These synergistic effects increase the grain size and improve the quality of $FASnI_3$ perovskite films. After the crystallization process, $ZnAc_2$ could uniformly encapsulate perovskite grains by forming a complex with $SnCl_2$ and an antioxidant (KHQSA) owing to the interaction between the Ac^- group and Sn^{2+}. This further enhances the air stability of the $FASnI_3$ perovskite layer. Thanks to the enlarged grain size and lowered defect density in perovskite films, the efficiency of $FASnI_3$ PSCs is improved from 6.70% to 8.38%.

The perovskite films were fabricated *via* one-step spin-coating of the perovskite precursor with different amounts of $ZnAc_2$. The reference perovskite precursor is composed of $FAPbI_3$ in a solvent mixture of DMF/DMSO with excess 7.0 mol% $SnCl_2$ and 1.5 mol% KHQSA, as reported in our previous work.[39] Fig. 1 shows the SEM images of perovskite films with the addition of different amounts of $ZnAc_2$. It can be observed that the grain size is gradually enlarged when increasing the amount of $ZnAc_2$ to 1.0 mol%. By further increasing the amount of $ZnAc_2$ to 3.0 mol%, the grain size is decreased and several holes appear in the films. In addition, no aggregates are formed in all films, suggesting that $ZnAc_2$ is uniformly dispersed in the films. Therefore, through the addition of a suitable amount of $ZnAc_2$, the grain size could be successfully enlarged and the morphology of $FASnI_3$ perovskite films could be optimized.

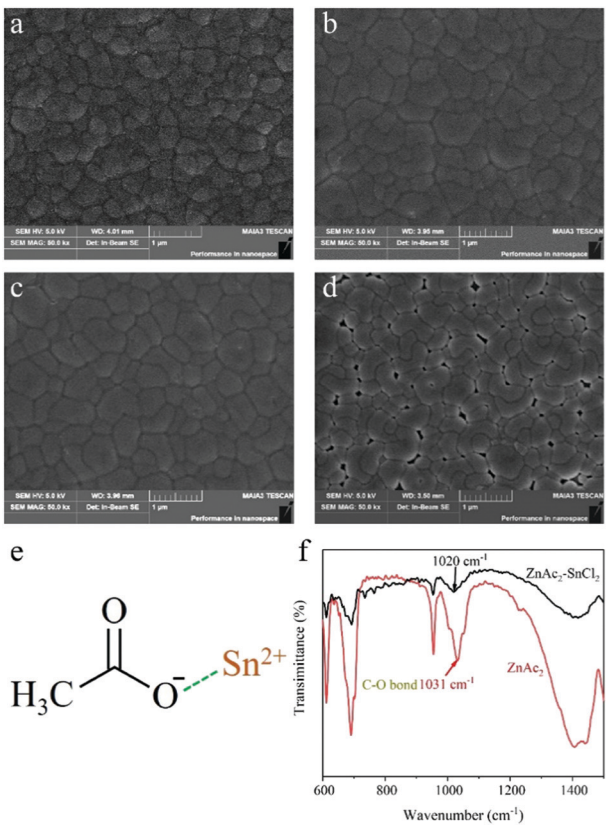

Fig. 1 SEM images of perovskite films without (a) and with 0.5 mol% (b), 1.0 mol% (c) and 3.0 mol% (d) $ZnAc_2$ addition. (e) The illustration of the interaction between the Ac^- group and Sn^{2+}. (f) FTIR patterns of $ZnAc_2$ and $ZnAc_2$–$SnCl_2$ complex powders.

It should be noted that a Lewis adduct could be formed between a Lewis base Ac^- and a Lewis acid Sn^{2+}, as shown in Fig. 1e. Fourier transform infrared (FTIR) spectroscopy characterization was employed to verify this interaction. Fig. 1f shows the FTIR patterns of $ZnAc_2$ and $SnCl_2$–$ZnAc_2$ composite powders, respectively. The C–O stretching vibration for pure $ZnAc_2$ is observed at 1031 cm^{-1}, while for $ZnAc_2$–$SnCl_2$ the C–O stretching vibration is shifted to a lower wavenumber of 1020 cm^{-1}.[42] This result confirms the interaction between the Ac^- group and Sn^{2+}. Hence, in the crystallization process, the formation of the FAI·SnI_2·$ZnAc_2$ intermediate phase could be due to the interaction between the Ac^- group and Sn^{2+}.[43] This intermediate phase could retard the crystallization process to enlarge the grain size.[26] Moreover, the introduction of Zn ions could affect the nucleation and subsequent crystal growth process, which also increased the grain size,[44,45] which is similar to the effect observed in lead-based perovskites with the introduction of Zn ions.[46] The deceased grain size and occurrence of holes with excessive $ZnAc_2$ addition could be ascribed to the steric effect of $ZnAc_2$, which separates the adjacent perovskite grains.[43]

X-ray diffraction (XRD) characterization was conducted on these films to study the effect of $ZnAc_2$ on the crystallinity of $FAPbI_3$ (see the ESI,† Fig. S1). The perovskite film with the addition of 1.0 mol% $ZnAc_2$ shows the highest intensity, indicating the high quality due to the large grains and better crystallinity. No peak shift is observed in all films, suggesting that Zn and Ac ions are not incorporated into the $FASnI_3$ lattice. This is because the molar ratio of FAI and SnI_2 is equal in the precursor and the Lewis acidity of Sn^{2+} is much stronger than that of Zn^{2+}. Zn ions are unable to substitute Sn^{2+} in $FASnI_3$ under this condition. Therefore, it is reasonable to assume that $ZnAc_2$ is uniformly dispersed at grain boundaries and surfaces in the crystallized perovskite films by forming a complex with $SnCl_2$ and the antioxidant (KHQSA). The pure $SnCl_2$ and $SnCl_2$–$ZnAc_2$ composite films were prepared and optical microscopic characterization was conducted to confirm this assumption (see the ESI,† Fig. S2). The pure $SnCl_2$ film is very rough due to the formation of branched crystals, while a uniform and smooth morphology is formed for the $SnCl_2$–$ZnAc_2$ composite film where the crystallization of $SnCl_2$ is significantly suppressed. Therefore, based on FTIR and optical microscopy characterization, it can be concluded that $ZnAc_2$ formed a complex with $SnCl_2$ and the antioxidant to encapsulate the perovskite grains in the crystalized films, which can further enhance the protection of Sn perovskites from oxidation.

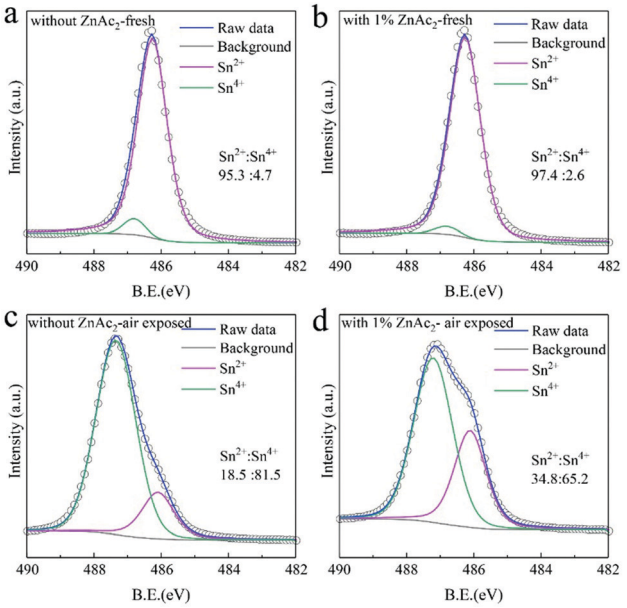

Fig. 2 XPS Sn $3d^{5/2}$ spectra of $FASnI_3$ films without (a and c) and with (b and d) 1.0 mol% $ZnAc_2$. All films were prepared with $SnCl_2$ and KHQSA as the basic conditions. Samples (a and b) were characterized under fresh conditions; Samples (c and d) were characterized after exposure to air for 12 h (RH20%).

X-ray photoelectron spectroscopy (XPS) characterization was performed to investigate the Sn^{4+} content in $FASnI_3$ films with and without the addition of 1% $ZnAc_2$. As shown in Fig. 2a and b, the Sn^{4+} content in fresh $FASnI_3$ is 4.7%, while it is decreased to 2.6% in fresh $FASnI_3$ with the introduction of 1.0 mol% $ZnAc_2$. This suggests that the formed intermediate phase could suppress the oxidation of Sn^{2+} in the crystallization process. Moreover, the slower color change of the precursor solution with increasing amount of $ZnAc_2$ further demonstrates that the presence of $ZnAc_2$ could enhance the stability of Sn^{2+} in the precursor (see the ESI,† Fig. S3).[47] For the Sn perovskite films exposed to air for 12 h, the Sn^{4+} content is 65.2% for the $ZnAc_2$ doped film, which is lower than the value (81.5%) for the pristine film. The better air stability is attributed to the much thicker encapsulation complex layer with the addition of $ZnAc_2$.

Fig. 3a shows the steady-state photoluminescence spectra of perovskite films with the addition of different amounts of $ZnAc_2$. It can be observed that the perovskite film with the addition of 1.0 mol% $ZnAc_2$ demonstrates the highest PL intensity, suggesting the lowest defect density, which results from the efficient suppression of Sn^{2+} vacancy. Further incorporation would lead to a lower PL intensity due to the formation of pinholes in the films shown by the SEM image in Fig. 1d. The carrier transport property of perovskite films was investigated by Hall effect measurements using the four-contact Hall bar method.[25] Fig. 3b shows the hole carrier density and mobility of $FASnI_3$ films with the addition of different amounts of $ZnAc_2$. The 1.0 mol% $ZnAc_2$ doped film exhibits a much lower hole carrier density and a higher hole mobility than the reference one. Therefore, the addition of $ZnAc_2$ could significantly improve the optoelectronic and charge transport properties of Sn perovskite films by efficiently suppressing the formation of Sn^{2+} vacancy and enhancing the film crystallinity.

The PSCs with the p-i-n structure of ITO/NiO_x/$FASnI_3$/PCBM/BCP/Ag, as shown in Fig. 4a, were fabricated to demonstrate the effect of $ZnAc_2$ on the photovoltaic performance of devices. 7.0 mol% $SnCl_2$ and 1.5 mol% KHQSA were added into the precursor as basic additives. Fig. 4b shows the photovoltaic performances of PSCs with the addition of different amounts of $ZnAc_2$. It can be observed that, by increasing the amount of $ZnAc_2$ to 1.0 mol%, the PCE could be improved gradually with overall enhancement in the parameters. This improvement should be attributed to the enlarged grain size and suppressed defect density (mainly Sn^{+2} vacancy). Excessive $ZnAc_2$ addition (3.0 mol%) leads to inferior performance due to the presence of pin-holes in the films. The champion device with 1.0 mol% $ZnAc_2$ could reach a PCE of 8.38% with a V_{oc} of 0.54 V, a J_{sc} of 22.49 mA cm^{-2} and an FF of 0.69. Negligible hysteresis is observed (see the ESI,† Fig. S4). In comparison, the control device demonstrates a PCE of 6.70% with a V_{oc} of 0.50 V, a J_{sc} of

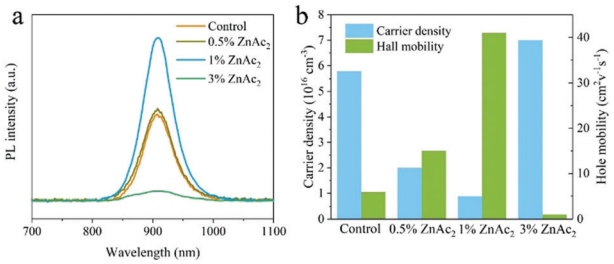

Fig. 3 (a) Steady-state photoluminescence spectra of Sn perovskite thin films deposited on glass substrates with the addition of different amounts of $ZnAc_2$. (b) Carrier density and carrier mobility of Sn perovskite films with the addition of different amounts of $ZnAc_2$ estimated from Hall effect measurements.

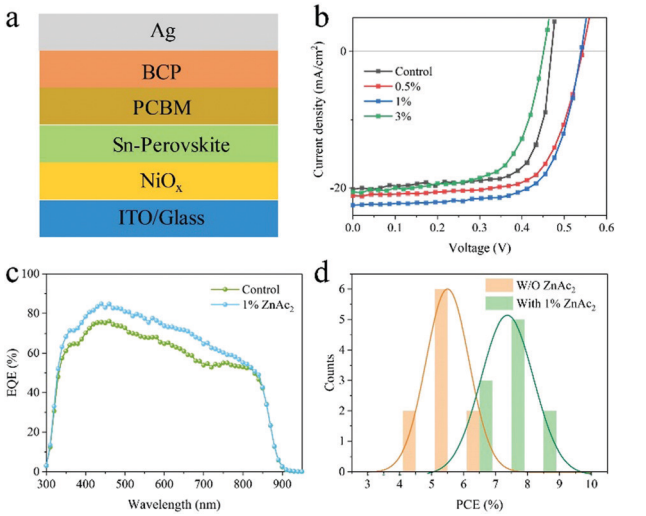

Fig. 4 (a) Schematic illustration of the device structure. (b) *J*–*V* cures of PSCs with the addition of different amounts of $ZnAc_2$. (c) EQE spectra of champion PSCs without and with 1.0 mol% $ZnAc_2$ addition, respectively. (d) The statistics of PCE distribution of 10 PSCs without and with 1.0 mol% $ZnAc_2$, respectively.

20.21 mA cm^{-2} and an FF of 0.67. The corresponding external quantum efficiency (EQE) spectra are presented in Fig. 4c. The calculated J_{sc} values are 19.24 mA cm^{-2} and 21.59 mA cm^{-2} for control and doped devices, respectively, which are close to the *J–V* measured values. The higher current density is attributed to the larger grain size and lower defect density with the introduction of $ZnAc_2$. Fig. 4d shows the statistics of PCEs of 10 devices with and without the addition of 1.0 mol% $ZnAc_2$. The average PCE for control devices is 5.5 ± 0.3%. Upon $ZnAc_2$ addition, the average PCE is increased to 7.25 ± 0.5%. This statistic verifies the positive effect of $ZnAc_2$ on the performance enhancement of Sn PSCs.

Conclusions

In summary, $ZnAc_2$ has been successfully employed to enlarge the grain size and decrease the defect density of $FASnI_3$ films. The improvement can be ascribed to the following reasons. First, the interaction between the Ac^- group and Sn^{2+} enables the formation of a $FAI{\cdot}SnI_2{\cdot}ZnAc_2$ intermediate phase, leading to an enlarged grain size and suppressed Sn^{2+} vacancy of $FASnI_3$ films. Besides, Zn ions could modify the nucleation to favor the crystal growth. Finally, $ZnAc_2$ could form a complex with $SnCl_2$ and the antioxidant to uniformly encapsulate the perovskite grains, which further strengthens the protection of perovskite films from oxidation. Consequently, the average efficiency of air-stable Sn PSCs has been improved from 5.5% to 7.25% with a relative enhancement of 31%. The efficiency of champion devices is improved from 6.70% to 8.38% with the addition of $ZnAc_2$. Our strategy provides a facile and compatible route to prepare air-stable Sn perovskite films with high quality, which can be expected to be applied in other optoelectronic devices.

Experimental

Materials

Formamidinium iodide ($CH(NH_2)_2I$) was purchased from GreatCell Solar; SnI_2 (99.999%), zinc acetate, nickel(II) nitrate hexahydrate ($Ni(NO_3)_2{\cdot}6H_2O$, 98%) and DMF (anhydrous, 99.8%) were purchased from Alfa Aesar. Bathocuproine (BCP, 96%), chlorobenzene (anhydrous, 99.8%), and DMSO (anhydrous, 99.9%) were purchased from Sigma-Aldrich. Phenyl-C71-butyric acid methyl ester ($PC_{71}BM$) was purchased from Nano-C Ltd.

Preparation of $SnCl_2$ and $SnCl_2$–$ZnAc_2$ powders

$SnCl_2$ was dissolved in DMSO with a 1 M molar weight. The $SnCl_2$–$ZnAc_2$ complex was prepared by dissolving $SnCl_2$ and $ZnAc_2$ in DMSO with 1 M and 0.5 M molar weights, respectively. Then the $SnCl_2$ and $SnCl_2$–$ZnAc_2$ solutions were spin-coated onto glass substrates, respectively, followed by thermal annealing at 100 °C to facilitate crystallization for 10 hours. Then the powders could be obtained by scraping the films from the substrates.

Device fabrication

ITO/glass substrates were sequentially washed with distilled water, acetone and isopropyl alcohol. Then, NiO_x films were prepared by spin-coating NiO_x solution by dispersing NiO_x nanocrystals in water as reported in our previous work.[39,41] The perovskite films were prepared by spin-coating the 0.8 M $FASnI_3$ precursor containing FAI, SnI_2, $SnCl_2$, KHQSA, and $ZnAc_2$ at a molar ratio of $1:1:0.07:0.015:x$ (x = 0, 0.005, 0.01, or 0.03) mixed in DMF/DMSO (13 : 1, v/v) at 5000 rpm for 30 s. During the spin-coating process, 90 μL of chlorobenzene was dripped on a rotating substrate at 10 s after starting. All perovskite films were annealed at 70 °C for 10 min. Next, electron transport layers (ETLs) were prepared by spin-coating a solution of PCBM in chlorobenzene (20 mg mL^{-1}) at 1500 rpm for 40 s. Bathocuproine (BCP, Sigma, 96%) dissolved in IPA (0.5 mg mL^{-1}) was spin-coated on the PCBM films at 4500 rpm for 30 s. Finally, devices were obtained with the evaporation of silver (Ag) top electrodes through a shadow mask. The area of the PSC is designed to be 4.8 mm^2.

Device characterization

Scanning electron microscopy (SEM) characterization was performed on a JEOL JSM 6335F SEM. X-ray diffraction measurements were performed using a Rigaku SmartLab X-ray diffractometer operating at room temperature. Time-resolved photoluminescence measurements of the samples were carried out by using an Edinburgh FLSP920 fluorescence spectrophotometer. A 485 nm laser was used as the excitation light source. Hall effect measurements were conducted using a four-probe Ecopia Hall Effect Measurement System (HMS-5000). FTIR spectroscopy was performed on a Bruker Vertex-70 in the attenuated total reflection mode. The current density ***versus*** voltage (*J–V*) characteristics of the PSCs were measured by using a Keithley 2400 source meter under the illumination of an AM 1.5 solar simulator with a light intensity of 100 mW cm^{-2} (Newport 91160, 300 W). The light intensity was calibrated with a standard silicon solar cell. The external quantum efficiencies of the PSCs were measured with a standard test system, including a xenon lamp (Oriel 66,02, 300 W), a Si detector (Oriel 76175_71580), a monochromator (Newport 66902) and a dual-channel power meter (Newport 2931_C).

Conflicts of interest

There are no conflicts to declare.

Acknowledgements

This work was financially supported by the Research Grants Council (RGC) of Hong Kong, China (Project No. PolyU 152068/18E).

References

1 M. Jeong, I. W. Choi, E. M. Go, Y. Cho, M. Kim, B. Lee, S. Jeong, Y. Jo, H. W. Choi, J. Lee, J.-H. Bae, S. K. Kwak, D. S. Kim and C. Yang, Stable perovskite solar cells with

efficiency exceeding 24.8% and 0.3-V voltage loss, *Science*, 2020, **369**, 1615–1620.
2 Y. Rong, Y. Hu, A. Mei, H. Tan, M. I. Saidaminov, S. I. Seok, M. D. McGehee, E. H. Sargent and H. Han, Challenges for commercializing perovskite solar cells, *Science*, 2018, **361**, eaat8235.
3 Y. Jiang, L. Qiu, E. J. Juarez-Perez, L. K. Ono, Z. Hu, Z. Liu, Z. Wu, L. Meng, Q. Wang and Y. Qi, Reduction of lead leakage from damaged lead halide perovskite solar modules using self-healing polymer-based encapsulation, *Nat. Energy*, 2019, **4**, 585–593.
4 S. Chen, Y. Deng, H. Gu, S. Xu, S. Wang, Z. Yu, V. Blum and J. Huang, Trapping lead in perovskite solar modules with abundant and low-cost cation-exchange resins, *Nat. Energy*, 2020, **5**, 1003–1011.
5 S. Wu, Z. Li, M.-Q. Li, Y. Diao, F. Lin, T. Liu, J. Zhang, P. Tieu, W. Gao, F. Qi, X. Pan, Z. Xu, Z. Zhu and A. K. Y. Jen, 2D metal–organic framework for stable perovskite solar cells with minimized lead leakage, *Nat. Nanotechnol.*, 2020, **15**, 934–940.
6 J. Li, H.-L. Cao, W.-B. Jiao, Q. Wang, M. Wei, I. Cantone, J. Lü and A. Abate, Biological impact of lead from halide perovskites reveals the risk of introducing a safe threshold, *Nat. Commun.*, 2020, **11**, 310.
7 X. Li, F. Zhang, H. He, J. J. Berry, K. Zhu and T. Xu, On-device lead sequestration for perovskite solar cells, *Nature*, 2020, **578**, 555–558.
8 X. Jiang, F. Wang, Q. Wei, H. Li, Y. Shang, W. Zhou, C. Wang, P. Cheng, Q. Chen, L. Chen and Z. Ning, Ultra-high open-circuit voltage of tin perovskite solar cells *via* an electron transporting layer design, *Nat. Commun.*, 2020, **11**, 1245.
9 C. Ran, W. Gao, J. Li, J. Xi, L. Li, J. Dai, Y. Yang, X. Gao, H. Dong, B. Jiao, I. Spanopoulos, C. D. Malliakas, X. Hou, M. G. Kanatzidis and Z. Wu, Conjugated Organic Cations Enable Efficient Self-Healing $FASnI_3$ Solar Cells, *Joule*, 2019, **3**, 3072–3087.
10 C. Wang, F. Gu, Z. Zhao, H. Rao, Y. Qiu, Z. Cai, G. Zhan, X. Li, B. Sun, X. Yu, B. Zhao, Z. Liu, Z. Bian and C. Huang, Self-Repairing Tin-Based Perovskite Solar Cells with a Breakthrough Efficiency Over 11%, *Adv. Mater.*, 2020, **32**, 1907623.
11 X. Meng, Y. Wang, J. Lin, X. Liu, X. He, J. Barbaud, T. Wu, T. Noda, X. Yang and L. Han, Surface-Controlled Oriented Growth of $FASnI_3$ Crystals for Efficient Lead-free Perovskite Solar Cells, *Joule*, 2020, **4**, 902–912.
12 T. Nakamura, S. Yakumaru, M. A. Truong, K. Kim, J. Liu, S. Hu, K. Otsuka, R. Hashimoto, R. Murdey, T. Sasamori, H. D. Kim, H. Ohkita, T. Handa, Y. Kanemitsu and A. Wakamiya, Sn(IV)-free tin perovskite films realized by *in situ* Sn(0) nanoparticle treatment of the precursor solution, *Nat. Commun.*, 2020, **11**, 3008.
13 T. Krishnamoorthy, H. Ding, C. Yan, W. L. Leong, T. Baikie, Z. Zhang, M. Sherburne, S. Li, M. Asta, N. Mathews and S. G. Mhaisalkar, Lead-free germanium iodide perovskite materials for photovoltaic applications, *J. Mater. Chem. A*, 2015, **3**, 23829–23832.
14 M. Chen, M.-G. Ju, H. F. Garces, A. D. Carl, L. K. Ono, Z. Hawash, Y. Zhang, T. Shen, Y. Qi, R. L. Grimm, D. Pacifici, X. C. Zeng, Y. Zhou and N. P. Padture, Highly stable and efficient all-inorganic lead-free perovskite solar cells with native-oxide passivation, *Nat. Commun.*, 2019, **10**, 16.
15 B.-W. Park, B. Philippe, X. Zhang, H. Rensmo, G. Boschloo and E. M. J. Johansson, Bismuth Based Hybrid Perovskites A3Bi2I9 (A: Methylammonium or Cesium) for Solar Cell Application, *Adv. Mater.*, 2015, **27**, 6806–6813.
16 M. Lyu, J.-H. Yun, M. Cai, Y. Jiao, P. V. Bernhardt, M. Zhang, Q. Wang, A. Du, H. Wang, G. Liu and L. Wang, Organic–inorganic bismuth (III)-based material: A lead-free, air-stable and solution-processable light-absorber beyond organolead perovskites, *Nano Res.*, 2016, **9**, 692–702.
17 P. C. Harikesh, H. K. Mulmudi, B. Ghosh, T. W. Goh, Y. T. Teng, K. Thirumal, M. Lockrey, K. Weber, T. M. Koh, S. Li, S. Mhaisalkar and N. Mathews, Rb as an Alternative Cation for Templating Inorganic Lead-Free Perovskites for Solution Processed Photovoltaics, *Chem. Mater.*, 2016, **28**, 7496–7504.
18 C. Zuo and L. Ding, Lead-free Perovskite Materials $(NH_4)_3Sb_2I_xBr_{9-x}$, *Angew. Chem., Int. Ed.*, 2017, **56**, 6528–6532.
19 C. C. Stoumpos, C. D. Malliakas and M. G. Kanatzidis, Semiconducting tin and lead iodide perovskites with organic cations: phase transitions, high mobilities, and near-infrared photoluminescent properties, *Inorg. Chem.*, 2013, **52**, 9019–9038.
20 I. Chung, J.-H. Song, J. Im, J. Androulakis, C. D. Malliakas, H. Li, A. J. Freeman, J. T. Kenney and M. G. Kanatzidis, $CsSnI_3$: Semiconductor or Metal? High Electrical Conductivity and Strong Near-Infrared Photoluminescence from a Single Material. High Hole Mobility and Phase-Transitions, *J. Am. Chem. Soc.*, 2012, **134**, 8579–8587.
21 M. Konstantakou and T. Stergiopoulos, A critical review on tin halide perovskite solar cells, *J. Mater. Chem. A*, 2017, **5**, 11518–11549.
22 Q. Tai, J. Cao, T. Wang and F. Yan, Recent advances toward efficient and stable tin-based perovskite solar cells, *EcoMat*, 2019, **1**, e12004.
23 T. Wang and F. Yan, Reducing Agents for Improving the Stability of Sn-based Perovskite Solar Cells, *Chem. – Asian J.*, 2020, **15**, 1524–1535.
24 K. Nishimura, M. A. Kamarudin, D. Hirotani, K. Hamada, Q. Shen, S. Iikubo, T. Minemoto, K. Yoshino and S. Hayase, Lead-free tin-halide perovskite solar cells with 13% efficiency, *Nano Energy*, 2020, **74**, 104858.
25 M. H. Kumar, S. Dharani, W. L. Leong, P. P. Boix, R. R. Prabhakar, T. Baikie, C. Shi, H. Ding, R. Ramesh, M. Asta, M. Graetzel, S. G. Mhaisalkar and N. Mathews, Lead-Free Halide Perovskite Solar Cells with High Photocurrents Realized Through Vacancy Modulation, *Adv. Mater.*, 2014, **26**, 7122–7127.
26 F. Hao, C. C. Stoumpos, P. Guo, N. Zhou, T. J. Marks, R. P. H. Chang and M. G. Kanatzidis, Solvent-Mediated Crystallization of $CH_3NH_3SnI_3$ Films for Heterojunction

Depleted Perovskite Solar Cells, *J. Am. Chem. Soc.*, 2015, **137**, 11445–11452.

27 F. Hao, C. C. Stoumpos, R. P. H. Chang and M. G. Kanatzidis, Anomalous Band Gap Behavior in Mixed Sn and Pb Perovskites Enables Broadening of Absorption Spectrum in Solar Cells, *J. Am. Chem. Soc.*, 2014, **136**, 8094–8099.

28 Z. Zhao, F. Gu, Y. Li, W. Sun, S. Ye, H. Rao, Z. Liu, Z. Bian and C. Huang, Mixed-Organic-Cation Tin Iodide for Lead-Free Perovskite Solar Cells with an Efficiency of 8.12%, *Adv. Sci.*, 2017, **4**, 1700204.

29 C. Ferrara, M. Patrini, A. Pisanu, P. Quadrelli, C. Milanese, C. Tealdi and L. Malavasi, Wide band-gap tuning in Sn-based hybrid perovskites through cation replacement: the $FA_{1-x}MA_xSnBr_3$ mixed system, *J. Mater. Chem. A*, 2017, **5**, 9391–9395.

30 W. Gao, C. Ran, J. Li, H. Dong, B. Jiao, L. Zhang, X. Lan, X. Hou and Z. Wu, Robust Stability of Efficient Lead-Free Formamidinium Tin Iodide Perovskite Solar Cells Realized by Structural Regulation, *J. Phys. Chem. Lett.*, 2018, **9**, 6999–7006.

31 E. Jokar, C.-H. Chien, C.-M. Tsai, A. Fathi and E. W.-G. Diau, Robust Tin-Based Perovskite Solar Cells with Hybrid Organic Cations to Attain Efficiency Approaching 10%, *Adv. Mater.*, 2019, **31**, 1804835.

32 W. Ke, C. C. Stoumpos, M. Zhu, L. Mao, I. Spanopoulos, J. Liu, O. Y. Kontsevoi, M. Chen, D. Sarma, Y. Zhang, M. R. Wasielewski and M. G. Kanatzidis, Enhanced photovoltaic performance and stability with a new type of hollow 3D perovskite $\{en\}FASnI_3$, *Sci. Adv.*, 2017, **3**, e1701293.

33 N. Ito, M. A. Kamarudin, D. Hirotani, Y. Zhang, Q. Shen, Y. Ogomi, S. Iikubo, T. Minemoto, K. Yoshino and S. Hayase, Mixed Sn–Ge Perovskite for Enhanced Perovskite Solar Cell Performance in Air, *J. Phys. Chem. Lett.*, 2018, **9**, 1682–1688.

34 S. J. Lee, S. S. Shin, J. Im, T. K. Ahn, J. H. Noh, N. J. Jeon, S. I. Seok and J. Seo, Reducing Carrier Density in Formamidinium Tin Perovskites and Its Beneficial Effects on Stability and Efficiency of Perovskite Solar Cells, *ACS Energy Lett.*, 2018, **3**, 46–53.

35 S. Shao, J. Liu, G. Portale, H.-H. Fang, G. R. Blake, G. H. ten Brink, L. J. A. Koster and M. A. Loi, Highly Reproducible Sn-Based Hybrid Perovskite Solar Cells with 9% Efficiency, *Adv. Energy Mater.*, 2018, **8**, 1702019.

36 I. Chung, B. Lee, J. He, R. P. Chang and M. G. Kanatzidis, All-solid-state dye-sensitized solar cells with high efficiency, *Nature*, 2012, **485**, 486–489.

37 M. E. Kayesh, T. H. Chowdhury, K. Matsuishi, R. Kaneko, S. Kazaoui, J.-J. Lee, T. Noda and A. Islam, Enhanced Photovoltaic Performance of $FASnI_3$-Based Perovskite Solar Cells with Hydrazinium Chloride Coadditive, *ACS Energy Lett.*, 2018, **3**, 1584–1589.

38 Z. Zhu, C.-C. Chueh, N. Li, C. Mao and A. K.-Y. Jen, Realizing Efficient Lead-Free Formamidinium Tin Triiodide Perovskite Solar Cells *via* a Sequential Deposition Route, *Adv. Mater.*, 2018, **30**, 1703800.

39 Q. Tai, X. Guo, G. Tang, P. You, T.-W. Ng, D. Shen, J. Cao, C.-K. Liu, N. Wang, Y. Zhu, C.-S. Lee and F. Yan, Antioxidant Grain Passivation for Air-Stable Tin-Based Perovskite Solar Cells, *Angew. Chem., Int. Ed.*, 2019, **58**, 806–810.

40 J. Cao, Q. Tai, P. You, G. Tang, T. Wang, N. Wang and F. Yan, Enhanced performance of tin-based perovskite solar cells induced by an ammonium hypophosphite additive, *J. Mater. Chem. A*, 2019, **7**, 26580–26585.

41 T. Wang, Q. Tai, X. Guo, J. Cao, C.-K. Liu, N. Wang, D. Shen, Y. Zhu, C.-S. Lee and F. Yan, Highly Air-Stable Tin-Based Perovskite Solar Cells through Grain-Surface Protection by Gallic Acid, *ACS Energy Lett.*, 2020, **5**, 1741–1749.

42 M. Jay Chithra, M. Sathya and K. Pushpanathan, Effect of pH on Crystal Size and Photoluminescence Property of ZnO Nanoparticles Prepared by Chemical Precipitation Method, *Acta Metall. Sin.*, 2015, **28**, 394–404.

43 T. Wu, X. Liu, X. He, Y. Wang, X. Meng, T. Noda, X. Yang and L. Han, Efficient and stable tin-based perovskite solar cells by introducing π-conjugated Lewis base, *Sci. China: Chem.*, 2020, **63**, 107–115.

44 Z. Zhang, W. Fan, X. Wei, L. Zhang, Z. Yang, Z. Wei, T. Shen, H. Si and J. Qi, Promoted performance of carbon based perovskite solar cells by environmentally friendly additives of CH_3COONH_4 and $Zn(CH_3COO)_2$, *J. Alloys Compd.*, 2019, **802**, 694–703.

45 R. Chen, D. Hou, C. Lu, J. Zhang, P. Liu, H. Tian, Z. Zeng, Q. Xiong, Z. Hu, Y. Zhu and L. Han, Zinc ion as effective film morphology controller in perovskite solar cells, Sustain, *Energy Fuels*, 2018, **2**, 1093–1100.

46 W. Zhao, D. Yang, Z. Yang and S. Liu, Zn-doping for reduced hysteresis and improved performance of methylammonium lead iodide perovskite hybrid solar cells, Mater. Today, *Energy*, 2017, **5**, 205–213.

47 R. Lin, K. Xiao, Z. Qin, Q. Han, C. Zhang, M. Wei, M. I. Saidaminov, Y. Gao, J. Xu, M. Xiao, A. Li, J. Zhu, E. H. Sargent and H. Tan, Monolithic all-perovskite tandem solar cells with 24.8% efficiency exploiting comproportionation to suppress Sn(ii) oxidation in precursor ink, *Nat. Energy*, 2019, **4**, 864–873.

